Carbohydrate Polymers 156 (2017) 86–96

Contents lists available at ScienceDirect

Carbohydrate Polymers

journal homepage: www.elsevier.com/locate/carbpol

Hyaluronan polymeric micelles for topical drug delivery

Daniela Šmejkalová[a], Tomáš Muthný[a], Kristina Nešporová[a,b,*], Martina Hermannová[a], Eva Achbergerová[a,c], Gloria Huerta-Angeles[a], Marek Svoboda[a,d], Martin Čepa[a], Veronika Machalová[a], Dominika Luptáková[e,f], Vladimír Velebný[a]

[a] Contipro a.s., Dolní Dobrouč, Czech Republic
[b] Institute of Experimental Biology, Faculty of Science, Masaryk University, Brno, Czech Republic
[c] Faculty of Technology, Department of Chemistry, Tomas Bata University in Zlín, Zlín, Czech Republic
[d] Department of Biological and Biochemical Sciences, Faculty of Chemical-Technology, University of Pardubice, Pardubice, Czech Republic
[e] Institute of Microbiology of the CAS, v.v.i., Prague, Czech Republic
[f] Department of Pharmacology, Jessenius Faculty of Medicine, Comenius University Bratislava, BioMed Martin, Slovakia

ARTICLE INFO

Article history:
Received 8 August 2016
Received in revised form 30 August 2016
Accepted 4 September 2016
Available online 5 September 2016

Keywords:
Skin penetration
Polymeric micelle
Hyaluronan

ABSTRACT

Nanosized materials offer promising strategy for topical drug delivery due to their enhancing effect on drug percutaneous transport across the *stratum corneum* barrier. In this work, polymeric micelles made from hydrophobized hyaluronic acid (HA) were probed for skin delivery. Compared to non-polymeric micelle solutions containing similar drug amount, *in vitro* skin penetration analysis indicated 3 times larger deposition of drug in the epidermis and 6 times larger drug deposition in the dermis after 5 h of topical treatment in Franz diffusion cells. The drug deposition was further increased with prolonged time of topical treatment. Laser confocal microscopy revealed the accumulation of both, the HA forming the vehicle and the payload, in the epidermis and dermis. Although fluorescent labeling of the HA would suggest co-transport of the HA and the drug, loading FRET pair dyes in the micellar core clearly demonstrated gradual micelle disruption with increasing skin depth. Transcellular penetration was the predominant pathway for the loaded drug. The HA polymeric micelles also demonstrated increased bioactivity of loaded compound *in vitro* and *in vivo*. In addition, the loaded micelles were found to be stable in cream formulations and thus they have great potential for topical applications for cosmetic and pharmaceutical purposes.

© 2016 Published by Elsevier Ltd.

1. Introduction

Nanosized materials such as liposomes, micelles, nanoparticles, nanoemulsions and polymeric suspensions are often reported to improve skin penetration of otherwise skin impermeable drugs into the *stratum corneum*, the topmost skin layer barrier (Karande & Mitragotri, 2009; Kong, Chen, Kweon, & Park, 2011; Lapteva, Mondon, Möller, Gurny, & Kalia, 2014; Lauterbach & Müller-Goymann, 2014; Yang, Bugno, & Hong, 2013). For this reason, colloidal nanosized systems have attracted great attention for topical administration of both cosmetically and pharmaceutically interesting compounds either for local or systemic delivery. At the same time, clinical applicability of the nanostructured systems as skin passive penetration enhancers is still under debate mainly due to the insufficient understanding of the interaction of nanosized drug delivery vehicles with the skin. This also includes limited knowledge about the fate and deposition of the vehicle material and drug in the skin layers after application (Wu, Price, & Guy, 2009). Compared to larger particles, nanosized systems are more likely to penetrate the *stratum corneum.* In this way, the nanoparticles have higher probability to access in the deeper skin layers including the circulatory system (Wu, Price, & Guy, 2009) and for this reason the health risk should be always assessed, mainly in case of long term skin exposure to nanosized systems (Bolzinger, Briancon, & Chevalier, 2011).

A number of attempts to make general rules regarding particle penetration from published results pointed out apparent inconsistences among the concluded observations (Bolzinger, Briancon & Chevalier, 2011; Contri, Fiel, Pohlmann, Guterres &, Beck, 2011; Prow et al., 2011). The reason for the data contradiction is probably the variety of nanomaterial constituents, used skin models and applied methodologies (Prow et al., 2011). The issue is quite complex and there is a number of potentially relevant parameters (Bolzinger, Briancon, & Chevalier, 2011). Besides the nanomate-

* Corresponding author at: Dolní Dobrouč 401, Dolni Dobrouč, Czech Republic.
E-mail address: kristina.nesporova@contipro.com (K. Nešporová).

http://dx.doi.org/10.1016/j.carbpol.2016.09.013
0144-8617/© 2016 Published by Elsevier Ltd.

rial size, other physico-chemical properties of the system including surface chemistry, shape, charge, amphiphilicity, porosity, aggregation and elasticity significantly affect interaction of nanomaterials with skin (Bolzinger, Briancon, & Chevalier, 2011; Yang, Bugno, & Hong, 2013).

To minimize the risk of non-biodegradable foreign particles accumulation in the body, a major area of polymer based drug delivery research is focused in the design of biodegradable polymer systems. Among these, hyaluronan (HA) represents an interesting material as topical drug delivery vehicle, especially in skin drug delivery, because HA is present in both the epidermis and dermis and constitutes a large fraction of skin extracellular matrix. In fact, the skin is believed to be a reservoir of about 1.7 g of HA, which is approximately one third of the total amount of HA expected to be present within the entire human body (Brown & Jones, 2005; Papakonstantinou, Roth, & Karakiulakis, 2012). HA is a natural polyanionic polysaccharide composed of repeating disaccharides that consist of *N*-acetyl-β-D-glucosamine and β-D-glucuronic acid linked by a 1 → 4 glycosidic bond. The disaccharides are linked by 1 → 3 bonds to form HA chain. HA hydrogels have been reported to be able to localize water soluble therapeutic agents in the superficial layers of the skin (Brown & Jones, 2005) and to improve protein drug delivery (Witting et al., 2015). Hyalurosomes, prepared from HA and soy phosphatidyl choline, improved curcumin deposition in the epidermis and dermis (Manca et al., 2015). Although there are still many questions regarding the mechanism of HA enhanced drug penetration, molecular weight and concentration of HA seem to play a crucial role in drug delivery. Regarding the delivery of hydrophilic drugs, shorter HA fragments (tens to hundreds of kDa) were more efficient in drug penetration (Brown & Jones, 2005; Cilurzo et al., 2014; Witting et al., 2015). Other factors, including active transport via HA receptors, specific structure of hydrated HA, and possible cotransport are also often discussed (Witting et al., 2015). HA in its native form contains hydrophobic patches formed in the secondary structure and so although being highly hydrophilic, it may non-covalently bind a limited amount of non-polar drugs (Scott, Cummings, Brass, & Chen, 1991). The binding capacity of HA for non-polar drugs may be enhanced by HA hydrophobization (Smejkalova et al., 2014), for example by esterification with fatty acids (Huerta-Angeles, Bobek, Prikopova, Smejkalova, & Velebny, 2014). The hydrophobized HA undergoes self-assembling in aqueous solutions while forming core-shell structures (polymeric micelles), where HA forms the hydrophilic shell, while the acyl chains aggregate in the hydrophobic core. This core may accommodate non-polar drugs through non covalent interactions.

Since both polymeric micelles and HA in its native form are often described as skin penetration enhancers (Witting et al., 2015; Yang, Bugno, & Hong, 2013), one would expect HA based micelles to improve skin penetration of hydrophobic drugs. To address this issue, two acylated derivatives of HA with short (hexyl HA, HAC6) and medium chain length (oleyl HA, HAC18:1) were prepared, transformed into polymeric micelles and at first loaded with Nile Red (NR) to simulate the hydrophobic active substance. The loaded micelles were topically (*in vitro*) applied to porcine skin and the fate of NR was followed and compared with control samples, qualitatively and quantitatively. In addition to the fate of loaded drug, we also tried to evaluate the penetration of the acylated HA, forming the drug delivery vehicle, by covalent labeling of acylated HA with Nile Blue and following its fluorescence signal in skin. Finally, the HA polymeric micelles were loaded with cosmetic active (coenzyme Q10), added in o/w cream formulations and tested for *in vivo* efficacy on human volunteers.

2. Materials and methods

2.1. Materials

Sodium hyaluronate (HA) (M_w = 15,000 g/mol) was provided by Contipro a.s. (Dolní Dobrouč, Czech Republic). Isopropanol (IPA), triethylamine (TEA), *cis*-oleic acid (C18:1), sodium chloride (NaCl), tetrahydrofurane (THF) and chloroform were obtained from Lach-ner (Czech Republic). Hexanoic acid (C6), benzoyl chloride (BC), 4-dimethylaminopyridine (DMAP), 4-acetamido-2,2,6,6-tetramethylpiperidine1-oxyl (4-Ac-TEMPO), disodium hydrogen phosphate ($NaHPO_4.12\,H_2O$), sodium bromide (NaBr), sodium hydroxide, sodium hypochlorite, Nile Red (NR) and Nile blue A (NB) are commercially available products from Sigma-Aldrich. 3,3′-dioctadecyloxacarbocyanine, perchlorate (DiO) and 1,1′-dioctadecyl-3,3,3′, 3′-tetramethylindocarbocyanine perchlorate (Dil) were obtained from Biotium Inc. (USA). Triglycerides (caprylic/capric triglyceride), glycerine, cream maker blend (glyceryl stearate, PEG-100-stearate), gel maker EMU (sodium acrylate, acryloyldimethyl taurate copolymer, isohexadecane, polysorbate 80), vitamin E acetate and benzyl alcohol for cream composition were purchased from MakingCosmetics (Snoqualmie, WA, USA). The cream composition consisted of 75.2% demineralized water, 12% triglycerides, 5% cream maker blend, 4% glycerine, 2% gel maker EMU, 1% vitamin E acetate and 0.8% benzyl alcohol.

2.2. Synthesis of oxidized hyaluronan (HA-ox)

HA (20.0 g, 50 mmol, M_w = 15,000 g/mol) was dissolved in water (1000 mL). Afterwards, sodium bromide (2.6 g, 25 mmol) and disodium hydrogen phosphate (38.8 g, 108 mmol) were added to the reaction mixture. The pH was adjusted to 9.0 with 0.1 M of sodium hydroxide. The solution was cooled to 5 °C for 2 h, bubbled with nitrogen and 4-Ac-TEMPO previously dissolved in 1 mL of water (106.7 mg, 0.5 mmol) was added. Finally, 6 mL of sodium hypochlorite (12.5 mmol) was added to the reaction. The oxidation was carried out for 15 min and stopped by adding 250 mL of isopropanol and diluted with water (1000 mL). The solution was ultrafiltered through a 5 kDa cut-off cassette (Merck-Millipore). The product was recovered after precipitation with isopropanol, decantation and dried in an oven at 60 °C for 24 h. The obtained degree of substitution (DS) of the aldehyde was 5.5 %, calculated by integration of the signal at 5.2 ppm with respect to the $-NH-COCH_3$ located at 2.1 ppm. Yield of the reaction was 86.5%. M_w of the product (SEC-MALLS): 15,800 g/mol and polydispersity: 1.6. FT-IR (KBr, cm^{-1}): 3419 (υ, C—OH), 2923, 1656, 1614 (—C=O), 1413 (-O—C=O), 1153, 1080 υ (C—OH), 1039, 607. ^{1}H NMR (500 MHz, NaOD): δ 2.1 (s, 3H, $-NH-COCH_3$), 3.4–4.0 (m, 10H, skeletal, CH), 4.4–4.6 (m, 2H, anomeric, CH), 5.2 (s, 1H,-$CH(OH)_2$).

2.3. Synthesis of oleyl hyaluronan grafted with Nile blue (HAC18:1-NB)

At first, oxidized HA (HA-ox) was grafted with Nile Blue, to produce HA-NB (Fig. S7). 500 mg of HA-ox (M_w: 15,800 g/mol and DS of 5.5%, 1.25 mmol) was dissolved in distilled water (25 mL). To that solution, Nile Blue (88 mg, 0.12 mmol), previously dissolved in 10 mL of DMSO was added. The reaction was allowed to react for 5 h at 25 °C in darkness. After that time, a reduction of the imine was carried out for 24 h at 25 °C by using $NaBH_3CN$ (78 mg, 1.25 mmol). After that time, the product was isolated by precipitation using excess of isopropanol (250 mL) and saturated NaCl solution, washed with anhydrous isopropanol (10 × 50 mL). The obtained precipitate was dissolved in demi-water and dialyzed (cut off 3.5 kDa) against 1% NaCl and 1% $NaHCO_3$ aqueous solution (2 × 5 L), distilled water (4 × 5 L). The product was isolated by freeze-drying.

The obtained degree of substitution of the grafted NB was 0.85%, calculated by integration of the signal at 2.8 ppm with respect to the $-NH-COCH_3$ located at 2.1 ppm. Yield of the reaction was 56%. ^1H NMR (NaOD, 500 MHz): δ 2.1 (s, 3H,-NH–$COCH_3$), 2.8 (m, 2H, C6-modified dimers), 3.4–4.0 (m, 10H, skeletal, CH), 4.4–4.6 (m, 2H, anomeric, CH).

In the second step, HA-NB was esterified with oleic acid (Fig. S7). 0.3 g of HA grafted with Nile Blue (HA-NB, 0.7 mmol) were solubilized in 20 mL of isopropanol: water (1:1), to that solution, the reagents were added in the following order, TEA (0.36 mL, 2.62 mmol), DMAP (5 mg, 0.038 mmol) and finally 0.59 mL (1.87 mmol) of oleic acid activated with benzoyl chloride (0.27 mL, 1.87 mmol) were added, and allowed to react for 3 h at room temperature in darkness. The product was isolated by precipitation with the addition of 2 g of NaCl and excess of isopropanol (100 mL). After that, the product was washed with isopropanol (50 mL), four times with 50 mL of isopropanol: water (85% v/v) and finally two more times with 50 mL of isopropanol. The white precipitate was dried in an oven at 40 °C for 24 h. Degree of substitution (DS): 10%. Yield of the reaction was 85%. The M_w was not determined due to high aggregation of the derivative. ^1H NMR (D_2O, 500 MHz): acyl signals: δ 0.9 (t, 3H, $-CH_2-CH_3$), 1.2-1.4 (m, 24H, $(-CH_2-)_{12}$), 1.6 (m, 2H, $-CH_2-CH_2-CO-$), 2.4 (t, 2H, $-CH_2-CO-$), 5.5 (m, 2H, CH=CH); HA signals: δ 2.0 (s, 3H, $-NH-COCH_3$), 3.4–3.9 (m, 10H, skeletal, CH), δ 4.4–4.6 (m, 2H, anomeric, CH).

2.4. Synthesis of sodium oleyl hyaluronan (HAC18:1)

HA (0.5 g, 1.25 mmol) was dissolved overnight in 10 mL of distilled water. To that solution, 5 mL of THF were slowly added, followed by TEA (0.52 mL, 3.75 mmol) and DMAP (8 mg, 0.063 mmol). In the second reaction flask, oleic acid (0.39 mL, 1.25 mmol) was activated with benzoyl chloride (0.15 mL, 1.25 mmol) in the presence of TEA (0.52 mL, 3.75 mmol) in THF (5 mL). The formation of the aromatic carboxylic anhydride was carried out for 30 min at 25 °C (Fig. S1). Then, that solution was added to the solution containing HA. The reaction was carried out for 2 h. The product was isolated by precipitation with the addition of 2 g of NaCl. After that, the product was washed with isopropanol (50 mL), four times with 50 mL of isopropanol: water (85% v/v) and finally two more times with 50 mL of isopropanol. The white precipitate was dried in an oven at 40 °C for 24 h. The degree of substitution (DS) was determined to be 10 % (in mol%, i.e. moles of fatty acid to moles of HA dimer), obtained by normalizing the integral of the anomeric proton HA signals (4.6–4.3 ppm) to 67 and reading the integral value at δ = 0.9 ppm corresponding to the terminal $-CH_3$ of fatty acid. ^1H NMR (D_2O, 500 MHz): acyl signals: δ 0.9 (t, 3H, $-CH_2-CH_3$), 1.2-1.4 (m, 24H, $(-CH_2-)_{12}$), 1.6 (m, 2H, $-CH_2-CH_2-CO-$), 2.4 (t, 2H, $-CH_2-CO-$), 5.5 (m, 2H, CH=CH); HA signals: δ 2.0 (s, 3H, $-NH-COCH_3$), 3.4–3.9 (m, 10H, skeletal, CH), 4.3–4.6 (m, 2H, anomeric, CH).

2.5. Synthesis of sodium caproyl hyaluronan (HAC6)

Synthetic procedure was similar to HAC18:1 (Fig. S1), except for the fact that instead of oleic acid, caproic acid (0.47 mL, 3.75 mmol) was activated with benzoyl chloride (0.43 mL, 3.73 mmol). The DS was determined from ^1H NMR spectra to be 60%. ^1H NMR (D_2O, 500 MHz): acyl signals: δ 0.8 (m, 3H, CH_3), 1.3 (m, 4H, γ, δ CH_2), 1.6 (m, 2H, β CH_2), 2.4 (m, 2H, α CH_2); HA signals: 2.0 (s, 3H, $-NH-COCH_3$), 3.4–3.9 (m, 10H, skeletal, CH), 4.4–4.6 (m, 2H, anomeric, CH).

2.6. Preparation of Nile Red (NR), coenzyme Q10 and FRET loaded polymeric micelles

NR loaded micelles were prepared by solvent evaporation method. 1 mg of NR was dissolved in chloroform and added to 10 mL of 1% HAC6 or HAC18:1 aqueous solution. The organic solvent was removed by rotary evaporation till a thin film was achieved. The dried film was further hydrated with 10 mL of water. Non-incorporated NR was removed by filtration (1 μm glass fiber syringe filter) and the resulting filtrate containing polymeric micelles was freeze-dried. Similar loading procedure was used for coenzyme Q10 loading, adding 6 mg of coenzyme Q10 dissolved in chloroform to 1% HAC6 or 13 mg of coenzyme Q10 dissolved in chloroform to 1% aqueous solution of HAC18:1. In case of FRET loading, 0.5 mg of each FRET dye was added to 1% of HAC18:1.

The amount of incorporated drug was determined from the drug content analyzed by supercritical fluid chromatography (SFC) with UV detection (coenzyme Q10) or fluorescence spectrometry (FRET dyes and Nile Red) as described later.

The loading capacity was determined according to the following equation:

$$\text{loading capacity(wt\%)} = \frac{\text{amount of loaded drug}}{\text{amount of loaded polymeric micelles}} \times 100 \quad (1)$$

2.7. Preparation of control solutions for in vitro skin penetration

Three types of control solutions were used in this study: (i) Nile Red (NR) dissolved in oleic acid oil, (ii) NR dissolved in a mixture of oleic acid oil and HAC6 or HAC18:1 and (iii) NR dispersed in PBS. The oil solution and PBS dispersion were prepared from stock solution (weighing 1 mg of NR) and diluting the stock solution till desired NR concentration (0.0010 or 0.0030 mg/mL) was reached. A mixture of oil and derivative was prepared by dissolving NR in oleic acid oil and diluting it with PBS till desired concentration was reached. The samples were homogenized by UP200S (Hielscher), equipped with S2 sonotrode using continuus mode and 80% amplitude for 5 min.

2.8. Supercritical fluid chromatography of coenzyme Q10

Coenzyme Q10 quantifications were performed using supercritical fluid chromatography with UV detection at 270 nm (Waters). Separation was carried out on Acquity SFC column TORUS 1-AA (130 Å, 1.7 μm, 3.0 × 100 mm) from Waters kept at 40 °C. The mobile phase was pumped at 2.0 mL min^{-1} and consisted from carbon dioxide: methanol = 97: 3. ABPR pressure was set to 2000 psi. Injection volume was 1 μL.

Polymeric micelles with incorporated coenzyme Q10 were dissolved in water: isopropanol = 1: 4 to a final concentration 0.5 mg mL^{-1} (w/v). After complete dissolution, coenzyme Q10 was extracted with isooctane: chloroform = 85: 15 (v/v). α-Tocopherol was used as an internal standard at a concentration of 50 μg mL^{-1}.

2.9. In vitro skin penetration

Skin penetration experiments were performed according to OECD guidelines in vertical Franz diffusion cells using full-thickness skin (approx. 1 mm) from porcine auricles donated by local slaughter house. The receptor was filled with PBS (pH 7.4) held at 37 °C, the excised tissue was clamped between donor and receptor with stratum corneum facing upward and exposing a diffusion area of 1 cm^2. After 30 min equilibration, the donor was slowly filled with 0.5 mL of control or polymeric micelle solution (c = 1 mg/mL) or control solutions (containing 0.0010 or 0.0030 mg/mL NR) and covered by Parafilm. After an application lasting 5 and 20 h, the cells were dismantled, the skin was washed with PBS and (i) freezed and cryo-

sectioned for further microscopic examination or (ii) used for NR extraction. Each sample was prepared in triplicate.

To quantify NR, epidermal and dermal samples were homogenized and extracted with acetonitrile: PBS solution (5:1, v/v). The samples were centrifuged (12 000*g*, 10 min) to remove solid particles and the extract was analyzed by HPLC Waters Acquity system equipped with Kinetex 5 u XB-C18 column (250 × 4,6 mm) held at constant temperature 30 °C and PDA detector set at 264 nm. The calibration curve was prepared from NR dissolved in acetonitrile:PBS (5:1, v/v) (A = 79350c, R^2 = 0.9993, LOD = 0.01 μg/mL LOQ = 0.03 μg/mL). All solutions were filtered through 0.22 μm pore nylone syringe filters before analysis. The injection volume was 15 μL. The chromatographic eluent consisted of binary phase of 0.1% (v/v) formic acid in water (A) and acetonitrile (B), which was pumped at 1.2 mL/min with the following gradient mode: B was held for 2.5 min at 80%, increased to 90% over 3.5 min, and held at 90% for next 2 min. The NR recovery was between 70 and 90% for all examined skin samples.

Skin surface washing with make-up removal solution was performed applying 5 times 0.5 mL of commercial make up removal solution, which was gently wiped by cotton pads.

2.10. In vitro *drug release*

In vitro release of Nile Red from polymeric micelles was evaluated using a dialysis technique. 20 mg of polymeric micelles were dispersed in 4 mL saline phosphate buffer (PBS) (pH 7.4, I = 0.15 M), placed in snake skin membranes (MWCO 3.5 kDa) and dialyzed against 100 mL of PBS while shaking in dark at 37 °C. The medium was refreshed after 2, 4, 8, 24 and 72 h. The drug concentration was determined by HPLC (for details see *in vitro* skin penetration) after its extraction from PBS by $CHCl_3$.

2.11. *Widefield and confocal microscopy (localization and FRET)*

Cryo-sectioned skin samples from *in vitro* penetration studies were visualized without mounting by widefield fluorescent microscope Ti-Eclipse (Nikon) using TRITC filter for NR fluorescence detection and bright field for basic morphology evaluation. Subcellular localization and FRET analysis was performed on confocal scanning microscope TCS SP8X (Leica Microsystems GmbH). Samples for penetration and fluorescence localization were fixed in 4% PFA for 15 min and mounted in ProLong Antifade medium w/o DAPI for nuclear staining (ThermoFisher Scientific) and visualized using optimal excitation and emission wavelength for individual fluorophores, for NR and HAC18:1-NB the argon laser (514 nm) was used and emission was detected at 555–636 nm, and for DAPI the 405 nm diode and detection at 430–490 nm was utilized. Samples for FRET efficiency evaluation were fixed in 4% PFA for 15 min and mounted in Mowiol. Images were acquired using argon laser (488 nm) excitation and HC PL APO CS2 63x/1.40 OIL immersion objective (Leica Microsystems GmbH) utilizing lambda scanning mode with 488 nm excitation and detection in the range of 493–640 nm using hybrid detector (HyD) with step size 3 nm and detection bandwidth 20 nm. LasX software was used to obtain spectral data in the selected regions of interest (ROIs), with each ROI being 2 μm × 10 μm in size. For calculation of the FRET ratio, described by the formula:

$$FRET_{ratio} = \frac{I_{DiI}}{I_{DiI} + I_{DiO}} \quad (2)$$

where I_{DiI} is fluorescence intensity at 565 nm and I_{DiO} at 501 nm, and data processing Origin software (OriginLab Corporation, USA) was used.

2.12. *MALDI mass spectrometry imaging*

Treated skin tissue samples with polymeric micelles ($c_{HAC18:1+coenzymeQ10}$ = 1 mg mL^{-1}) and control skin tissue samples were sectioned into 20 μm thin slices using a cryostat (Leica CM 1950) at −25 °C. Sections were mounted onto ITO glass slide (Bruker Daltonics, Germany) in three technical replicates and vacuum-dried in a desiccator for 30 min. Standard coenzyme Q10 solution was spotted close to the tissue samples for semi-quantitation of coenzyme Q10 in the tissues. For the measurement, CHCA matrix (7 mg mL^{-1} dissolved in 0.2% TFA in water: acetonitrile = 1:1) was applied by ImagePrep (Bruker Daltonics, Germany) matrix deposition device using the default method.

All spectra were acquired by Solarix FTICR 12T (Bruker Daltonics, Germany) mass spectrometer equipped with Bruker smartbeam-II™ laser in positive ion mode. The lateral resolution was set to 50 μm, 200 laser shots were applied per position and 4 scans averaged per pixel. MSI data were processed and analyzed by FlexImaging 4.1 software (Bruker Daltonics, Germany).

2.13. *Cryo SEM analyses (micellar size and shape)*

To estimate polymeric micelle size, 20 mg of freeze dried micelles were gently dispersed in 0.4 mL of distilled water. 2–3 μL of the prepared solution were transferred in an Al target plate, immersed in liquid nitrogen and then transferred into cryochamber Alta 2500 (gatan). The samples were further coated with Pt/Pd mixture for 0.5 min, and analyzed at −135 °C by JEOL 7401F operating at an acceleration voltage 2 kV (gentle beam mode), current density 20 μA and 8 mm working distance from detector. The images were recorded in digital mode.

2.14. *Dynamic light scattering analyses (DLS)*

The hydrodynamic size and zeta potential of coenzyme Q10-loaded HA micelles (c = 0.5 mg/mL in saline phosphate buffer (PBS) pH 7.4) was determined at 25 °C using Zetasizer Nano-ZS fom Malvern Instrument equipped with a 633 nm He-Ne laser using back scattering detection.

2.15. *Golden-gate ATR*

ATR FTIR spectra of skin samples were collected using Thermo Nicolet Nexus 870 FTIR Spectrometer (Madison, WI, USA). MKII Golden Gate™ Heated Diamond ATR Top-Plate single reflection system (Specac Ltd, Orpington, Great Britain) was applied for the measurements of spectra of the samples. The spectra were collected in a range of 650–4000 cm^{-1} with liquid nitrogen cooled MCT (mercury cadmium telluride) detector using 256 scans, resolution 4 cm^{-1}, Happ-Genzel apodization and KBr beamsplitter.

2.16. *Size exclusion chromatography coupled to multi-angle laser light scattering (SEC-MALLS)*

SEC was performed using a Waters Alliance liquid chromatograph (Model e2695) equipped with refractive index detector (Model 2414, Waters) and a TREOS multi-angle laser light scattering photometer (Wyatt Technology Corporation). The injection volume was 100 μL of 1.0% w/v HA-derivative solutions. The separation was carried out using PL aquagel-OH 40 (300 × 7.5 mm; 8 μm) and PL aquagel-OH 20 (300 × 7.5 mm; 5 μm) columns connected in series. Columns were thermostated at 40 °C. The mobile phase was 0.1 M sodium phosphate buffer (pH adjusted to 7.5) + 0.05% NaN_3 at a flow rate 0.8 mL min^{-1}. Data acquisition and molecular weights calculations were performed using the ASTRA V software (Wyatt Technology Corporation, USA). The specific refractive index

increment dn/dc of 0.155 mL g^{-1} was used for the determination (Podzimek, Hermannova, Bilerova, Bezakova & Velebny, 2010).

Each sample was filtered through Acrodisc Syringe Filter 0.45 μm 25 mm diameter with the Supor membrane (Pall). All reagents for SEC were HPLC grade and the mobile phase was filtered through Nylaflo Nylon Membrane Filter 0.2 μm, 47 mm diameter (Pall).

2.17. Nuclear magnetic resonance (NMR)

^{1}H NMR spectra were recorded using a BRUKER Avance™ III 500 instrument operating at frequency of 500.25 MHz ^{1}H. The ^{1}H chemical shifts were referenced to 3-(trimethylsilyl)-propionic acid sodium salt used as internal standard. Acylated HA derivatives (8 mg) were dissolved in 750 μL of D_2O, transferred into NMR tubes and analyzed at 25 °C. Degree of substitution (DS) was expressed as the average percentage of modified HA dimers within the HA polymer. DS = 10% means, that 10 out of 100 dissacharide units were modified. The DS was determined from integral value of CH_3 signal resonating at 0.9 ppm and belonging to acyl chain, while normalizing integral intensity of anomeric H signals (4.6–4.3 ppm) belonging to HA to 67.

2.18. Fourier transform infrared spectroscopy (FTIR)

Infrared spectra of HA derivatives were measured using an FTIR-8400S Shimadzu spectrometer and KBr pellets method. 64 Scans were collected for each sample within the range of 400–4000 cm^{-1}.

2.19. In vitro *antioxidant activity*

WS-1 human fibroblasts (ATCC® CRL-1502™) were obtained from ATCC and cultivate in DMEM medium supplemented with 10% fetal bovine serum (Sigma Aldrich). Cells were seeded in 96 well plate (7000 cells per well) and let to adhere for 24 h (37 °C, 5% CO_2, 95% humidity). Adherent cells were pretreated by tested substances (coenzyme Q10 in DMSO, coenzyme Q10 loaded in HA-C18:1 micelles, HAC18:1 and DMSO) for 24 h. After pretreatment 100 μM H_2O_2 was added to cells for 30 min. Cells were then labelled with 1 μM JC-1 (AAT Bioquest) in serum free medium for 20 min in dark, washed with PBS and fluorescence was detected at Ex/Em = 490/525 nm and 490/590 nm for ratio analysis using EnSight plate reader (Perkin Elmer). H_2O_2 untreated cells were used as reference sample for relative quantification.

2.20. In vivo *efficacy test of cream formulation*

A double-blind randomized placebo-controlled study was performed on healthy volunteers (Caucasian type) according to the principles of the Declaration of Helsinki of World Medical Association. Volunteers were divided into four groups as follows and treated for 28 days: control group (n = 15; age 24–63 years, 32 in average; total dose 0 + 0 mg), HAC18:1 group (n = 7; age 25–43 years, 31 in average; total dose 20 + 0 mg), Coenzyme Q10 group (n = 6; age 25–51 years, 35 in average; 0 + 3 mg), and HAC18:1 + coenzyme Q10 group (n = 6; 25–51 years, 35 in average; 20 + 3 mg). Skin parameters were determined using multiprobe adapter system cutometer dual MPA 580 equipped with several probes (Courage-Khazaka electronic, Cologne, Germany). Skin elasticity was assessed using the cutometer probe and the elastic parameters were calculated from the obtained graphs. Skin gloss was determined by a GL 200 glossymeter, melanin and erythema by an MX 18 mexameter. Wrinkles were evaluated using a 3D LifeViz stereovision camera (QuantifiCare, San Mateo, CA, USA) providing 3D images of the skin. The pictures were analyzed with a LifeViz reconstruction image management software (QuantifiCare, San Mateo, CA, USA) to determine depth of wrinkles.

3. Results

3.1. Synthesis of HA derivatives

All HA derivatives used in this study were characterized prior their usage for polymeric micelle formation. Detailed information about structural analysis obtained by NMR and/or FTIR spectroscopy can be found in Materials and Methods. The derivatives were prepared from low molecular weight HA (M_w = 15,000 g/mol) with a maximum degree of substitution (DS) 10%, so that final products were well soluble in water and had low viscosity (i.e. could easily aggregate in aqueous solutions while forming polymeric micelles). Derivatives with larger M_w or DS did not fulfill these requirements and thus were avoided. Although one would expect derivatives having smaller M_w to be more efficient in topical delivery, such HA derivatives were not prepared, due to low reaction yields (a large amount of material is lost during purification), high production cost and thus industrial incompatibility.

3.2. Polymeric micelle characterization

Hyaluronan polymeric micelles were loaded with Nile Red (NR) by solvent exchange method. As shown in Fig. S2, both hexyl (HAC6) and oleyl (HAC18:1) hyaluronan polymeric micelles had spherical shapes. When dispersed in saline phosphate buffer (PBS), the average hydrodynamic size of loaded HAC6 was 234 nm with polydispersity of 0.2. At the same time, two size fractions (and thus high polydispersity index PDI of 0.5) having average hydrodynamic diameters of 21 and 122 nm were estimated for HAC18:1 (Fig. S3). The first peak could be assigned to single micelles, while that at larger diameter can be thought to arise from micelle aggregation. It is interesting that single micelles were not noted in case of HAC6. The smaller hydrodynamic size of HAC18:1 polymeric micelles may suggest a more compact structure comparing to HAC6. The zeta potential ranged from −25 to −27 mV (Table 1), indicating relatively stable vehicles. The loading capacity for NR was only about 0.1 and 0.3 wt.% for HAC6 and HAC18:1, respectively (Table 1). However, due to the strong fluorescent signal of NR, even such a low loading capacity was sufficient for the purpose of this study. Comparing the emission spectra of loaded NR in HAC6 and HAC18:1 (Fig. S4), the maximum emission fluorescence wavelength was 652 and 648 nm, respectively, indicating slightly more non-polar environment within the aggregated HAC18:1. The *in vitro* release of NR from polymeric micelles was found to be extremely slow and indicated that there is no burst release of the loaded compound up to 24 h from micelle dispersion in PBS (Fig. S5).

Table 1
Hydrodynamic size and polydispersity index (PDI) of HA polymeric micelles (HAC6 and HAC18:1) loaded with NR and coenzyme Q10 (coQ10) at 0.5 mg/mL in PBS (pH 7.4).

Sample + loaded compound	Loading capacity (wt.%)	Hydrodynamic diameter (nm)	PDI	Zeta potential (mV)
HAC6 + NR	0.1	234	0.2	−25.1
HAC18:1 + NR	0.3	21 and 122[a]	0.5	−26.8
HAC6 + coQ10	2.5	192	0.1	−25.1
HAC18:1 + coQ10	11.3	163	0.1	−25.6

[a] bimodal distribution.

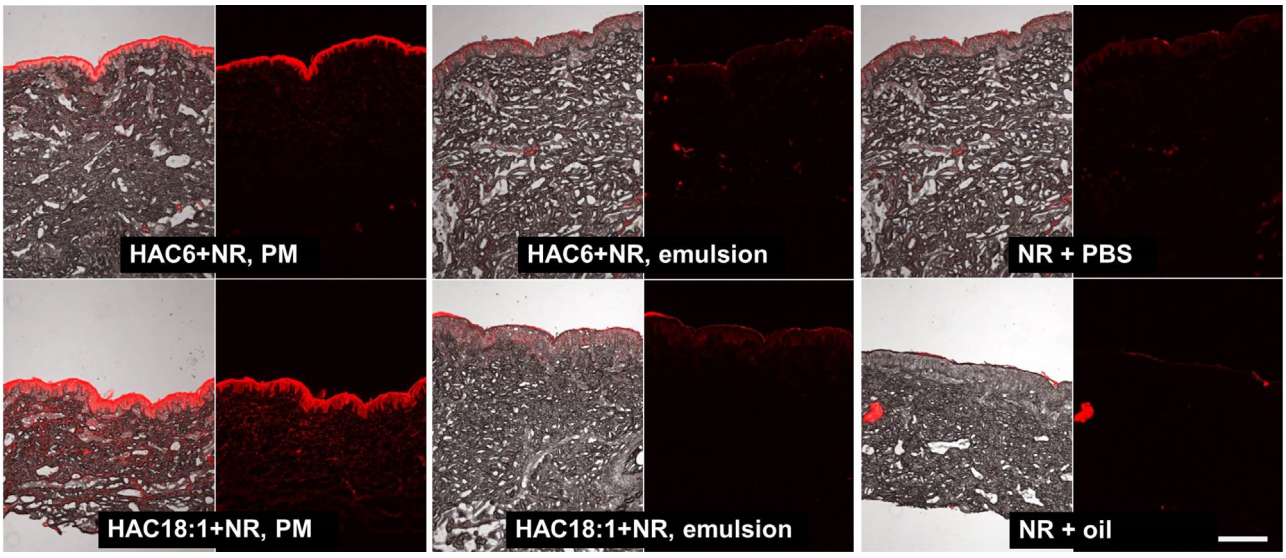

Fig. 1. Cross sectional images of porcine skin after 20 h treatment with NR loaded in HAC6 and HAC18:1 polymeric micelles (PM), NR mixed with HAC6 and HAC18:1 in an emulsion and NR dissolved in oil and dispersed in PBS. Scale bar = 200 μm.

3.3. *Effect of HA polymeric micelles on skin penetration*

The effect of HA polymeric micelles on NR penetration was studied comparing qualitative and quantitative data obtained after passive penetration of NR loaded in polymeric micelles (HAC6, HAC18:1) and control solutions. The control solutions, containing the same amount of NR as the HA micelles, consisted of NR dissolved in (i) oleic acid oil, (ii) dispersed in PBS, and dissolved in a (iii) mixture of oil and HAC6 or HAC18:1 derivative (o/w emulsion), where NR was not encapsulated in the micelle core. The confirmation of NR encapsulation or its non-encapsulation was performed by a simple extraction test mixing the tested aqueous solution with chloroform (1:1 v/v). Encapsulated NR in polymeric micelles cannot be extracted under these conditions in organic phase because the micelles remain intact and they protect NR from the surrounding solvent. At the same time, free (unencapsulated) NR is easily transferred to chloroform phase.

Fig. 1 shows fluorescent microscopic images of cross-sections of porcine skin treated with the polymeric micelles and control solutions. The images demonstrate that NR loaded in polymeric micelles penetrated more efficiently into the *stratum corneum*, epidermis and dermis when compared to the controls, where NR fluorescence was much weaker and rather restricted in the superficial epidermal layers. To quantify the amount of the penetrated NR, the porcine skin (exact area of 1 cm^2) was removed after 5 and 20 h of incubation from Franz cells, washed with PBS and separated into the epidermis (containing the *stratum corneum*) and dermis, out of which Nile Red was extracted. The *stratum corneum* was not separated from viable epidermis to minimalize manipulation with skin sample and shorten the time needed for NR extraction. Compared to the NR deposition from control solutions, the detected amount of NR from HA polymeric micelles was found to be 3 times larger in the epidermis and 6 times larger in the dermis, after 5 h of incubation (Fig. 2). Within the next 15 h of incubation, the amount of NR delivered from polymeric micelles to the dermis was further tripled, while the NR content in the epidermis remained constant. Despite the variation in hydrodynamic sizes and polymeric micelle polydispersity (Table 1), no significant difference was noted between quantitative delivery of NR by HAC6 and HAC18:1 polymeric micelles. Among the control solutions, the largest penetration of NR in the skin was observed from PBS suspension. However, only about 10% of the total NR content in PBS suspension placed on the skin surface (as donor in Franz cells) was able to penetrate the stratum corneum, while about 45% of NR was delivered to deeper skin layers in case of HA polymeric micelles (Fig. 2). NR levels in the receptor compartment were below the limit of quantification, and thus the risk of drug access to the circulatory system is rather low.

To confirm penetration of NR from HA polymeric micelles in deeper skin layers, the porcine skin incubated with control and HA micelle solution was washed with PBS and afterwards cleaned with make-up removal solution. As it is evident from Fig. S6, the make-up removal solution removed almost all NR in the control skin sample (incubated with NR emulsion) while a strong NR fluorescence remained in the skin sample treated with polymeric micelles.

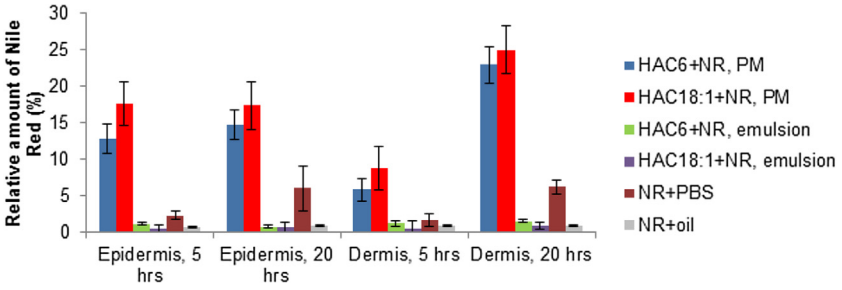

Fig. 2. Determination of NR amount in epidermis and dermis after its skin extraction (n = 3). The porcine skin was treated 5 and 20 h with NR loaded in HAC6 and HAC18:1 polymeric micelles (PM), NR mixed with HAC6 and HAC18:1 in an emulsion and NR dissolved in oil and dispersed in PBS.

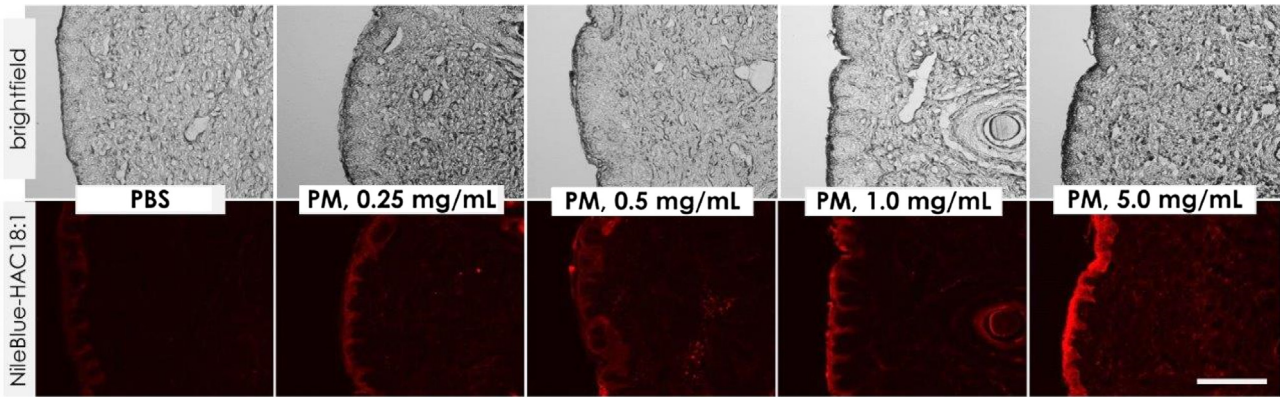

Fig. 3. Cross sectional images of porcine skin after 20 h treatment with (i) PBS and (ii) HAC18:1 polymeric micelles (PM) covalently labeled with Nile Blue (HAC18:1-NB), topically applied at different concentrations (0.25, 0.5, 1.0 and 5.0 mg/mL). Scale bar = 200 μm.

3.4. Fate of HA polymeric micelle

To estimate the fate of HA forming the vehicle, HA was covalently labeled with Nile blue (NB), subsequently acylated and transformed into polymeric micelles (not loading any hydrophobic compound) and evaluated for skin penetration. The reaction scheme is shown in Fig. S7, the DS of the final product HAC18:1-NB was <1%, and 10% for Nile Blue and oleyl, respectively. The fluorescence images (Fig. 3) of the cross-sectioned skin demonstrated increasing fluorescence intensity in the epidermis and dermis with increasing concentration of the HAC18:1-NB solution used to treat the skin for 20 h. Thus, the modified HA is able to penetrate through the *stratum corneum* into deeper skin layers. For a more detailed information, confocal images were taken from skin samples treated with (i) empty (i.e. non-loaded) HAC18:1-NB polymeric micelles and (ii) HAC18:1 polymeric micelles loaded with Nile Red (Fig. 4). The images again confirm that both the loaded NR and HA forming the vehicle penetrate the stratum corneum. When the cell nuclei were stained with Hoechst blue (Fig. 4) the red fluorescence from both the loaded and unloaded micelles were detected in the cytoplasm surrounding the cell nuclei in epidermal and dermal layers. Enlargement of the *stratum corneum* in Fig. S8 further indicates transcellular pathway, because NR signal was detected both across and through the corneocytes.

The loaded polymeric micelle could enhance penetration of the loaded drug across the stratum corneum while losing its aggregation or it could penetrate as an entity (entire loaded vehicle) and subsequently release its payload in deeper skin layers. To evaluate this, polymeric micelles were loaded with a Förster resonance energy transfer (FRET) pair dyes, DiI, a red-orange fluorescent lipophilic probe as an acceptor, and DiO, a green fluorescent lipophilic probe as a donor, and the polymeric micelles were left to penetrate skin in Franz diffusion cells. Close proximity of the two dyes in the micelle core results in efficient FRET effect. Release of core-loaded molecules leads to an increased distance between the fluorescent molecules, and thus reduction in FRET efficiency (Chen et al., 2008). The FRET efficiency was evaluated calculating FRET ratio $I_{DiI}/(I_{DiI} + I_{DiO})$, which was estimated to be 0.84 for intact (dissolved in PBS) and 0.40 for disrupted (dissolved in acetonitrile: PBS 5:1 v/v) micelles, respectively. As it is reported in Fig. 5, the FRET ratio observed from cross section skin images was decreasing with increasing skin depth, thus suggesting progressive micelle disruption.

3.5. Interaction of HA polymeric micelles with the stratum corneum

HA was previously reported to promote changes in the secondary structure of keratin, inducing conversion of α-helical structure in β-sheet structure (Witting et al., 2015). These changes are detectable in FTIR spectra and are connected with decreased skin barrier function and HA penetration in deeper skin layers (Kaushik, Costache & Michniak-Kohn, 2010; Witting et al., 2015). However, in our case, there were no changes detected in FTIR spectra of control skin sample and sample treated with HA polymeric micelles (Fig. S9), both in the region of α-helical (1650 cm^{-1}) and β-sheet protein structures. Nor were there any changes noted in the region of 2700–3100 cm^{-1} attributed to the vibration of intercellular lipids. These results indicate that HA polymeric micelles did not significantly alter the structural organization of skin lipids and proteins in the *stratum corneum*.

3.6. Coenzyme Q10 loaded in HA polymeric micelles

A possible application of polymeric micelles is their incorporation in cream formulations. As it is shown in Fig. S10, there is still enhanced penetration of NR from HA polymeric micelles compared to the control cream formulations with none or free NR. Due to this fact, NR was substituted with a more attractive compound for topical applications – coenzyme Q10, which was loaded in HAC6 and HAC18:1 derivatives. Coenzyme Q10 is a highly lipophilic substance with limited topical bioavailability (Lee & Tsai, 2010), in the skin it serves as antioxidant and energy transfer molecule. The level of coenzyme Q10 has been reported to decline between the ages of 30 and 80 years, and thus exogenous delivery of coenzyme Q10 in epidermis represents a great potential. The loading capacity of HAC6 and HAC18:1 was about 2.5 and 11 wt.%, respectively. The loaded micelles dispersed in PBS had narrow polydispersity (PDI = 0.1) with average hydrodynamic diameter of 190 and 160 nm (Table 1). HAC18:1 had better structural compatibility with coenzyme Q10, and thus larger loading capacity, further experiments were made only for this type of micelle dispersion. Since coenzyme Q10 cannot be followed in skin samples due to its low fluorescence intensity, its *in vitro* skin delivery was followed by MALDI Mass Spectrometry Imaging. As it is shown in Fig. 6, very weak signal of protonated coenzyme Q10 (m/z 863.691) was detected in control sample. The control sample was treated only with PBS, and so the detected coenzyme Q10 was naturally occurring coenzyme in skin. At the same time, significant coenzyme Q10 skin enrichment was detected in the upper epidermis when HAC18:1 polymeric micelles were applied.

HAC18:1 polymeric micelles loaded with coenzyme Q10 were at first tested for their *in vitro* protective antioxidant activity on WS1 human fibroblasts (Fig. S11). In this experiment the skin cells were cultivated with HAC18:1, free coenzyme Q10, and coenzyme Q10 loaded in HAC18:1 for 24 h, followed by induction of oxidative stress caused by treatment with H_2O_2. The oxidative damage was

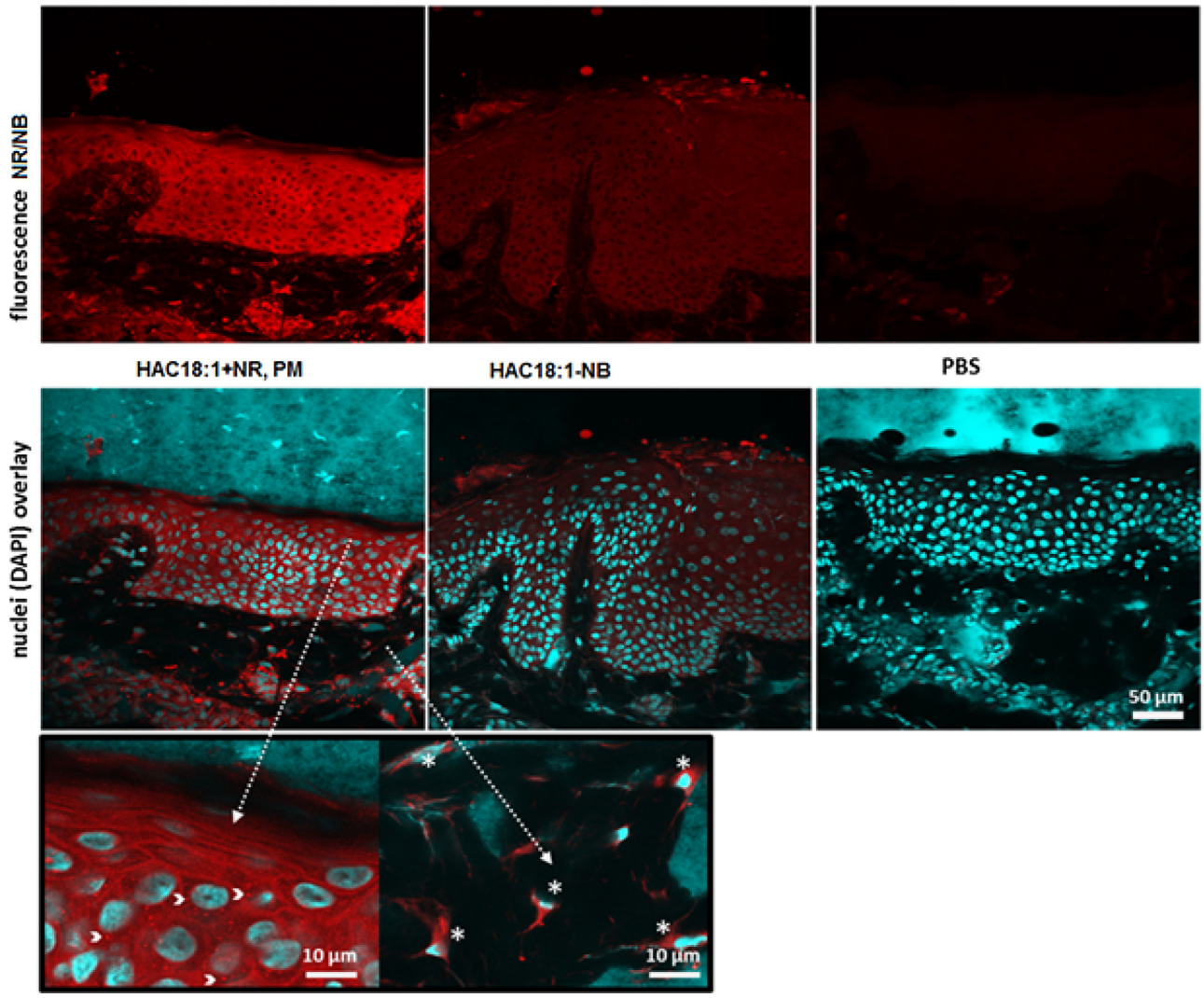

Fig. 4. Confocal images of cross sections of porcine skin after 20 h treatment with (i) PBS (=control) and (ii) HAC18:1 polymeric micelles loaded with NR (HAC18:1 + NR, PM) and (iii) HAC18:1 polymeric micelles not loaded with any drug but covalently labeled with Nile Blue (HAC18:1-NB). Both NR and NB appear with red fluorescence. Bottom pictures show merged images of NB or NR fluorescence and stained cell nuclei (blue). Details (in black frame) of skin sample treated with NR loaded micelles-keratinocytes with vesicle (arrows) on the left and dermal fibroblasts (*) on the right. (For interpretation of the references to colour in this figure legend, the reader is referred to the web version of this article.)

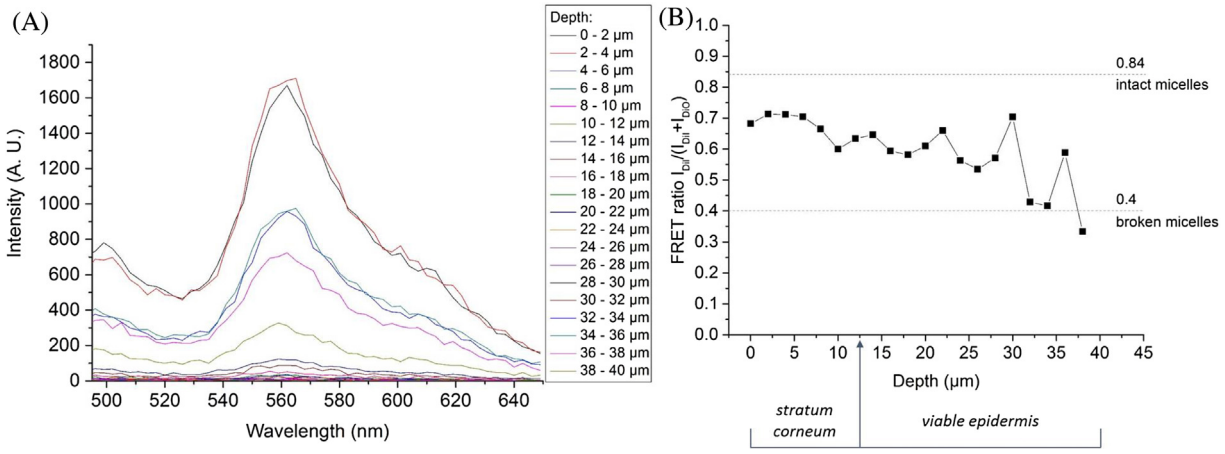

Fig. 5. Emission spectra of HAC18:1 + FRET polymeric micelles as a function of different skin depth (A) and the corresponding FRET ratio (B).

quantified from the ratio of fluorescence intensities, observed after JC-1 labeling. Intact mitochondrial membrane is characterized by red fluorescence, while green fluorescence is typical for decreased mitochondrial potential. This *in vitro* assessment of protective anti-

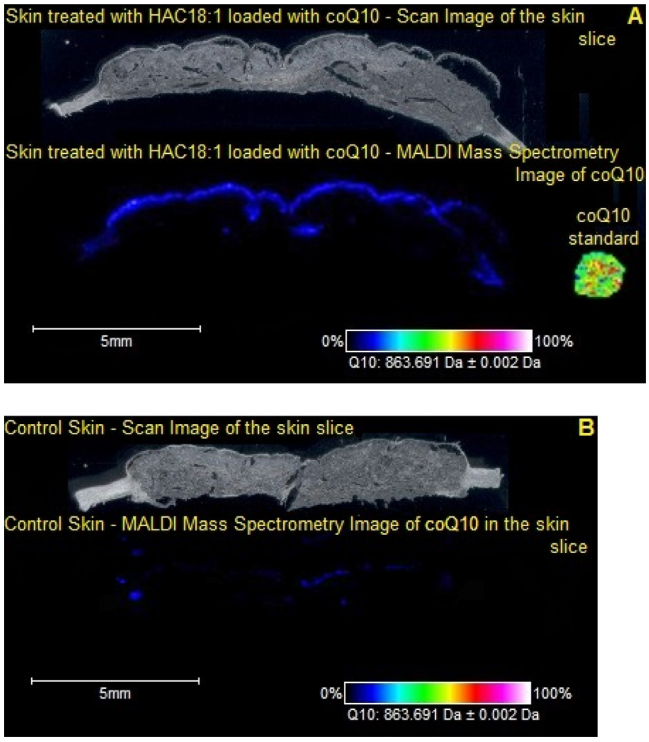

Fig. 6. MALDI Mass Spectrometry Imaging of coenzyme Q10 (coQ10) of porcine skin treated for 20 h with HAC18:1 polymeric micelles loaded with coQ10 at concentration 1 mg mL^{-1} (A) and with PBS (B). Furthermore, MALDI Mass Spectrometry Image of coQ10 standard spotted close to the tissue is superimposed in A.

oxidative activity of coenzyme Q10 showed that only coenzyme Q10 loaded in HA-C18:1 micelles was able to prevent the negative change in mitochondrial potential after peroxide treatment of skin cells. The same concentrations of HA-C18:1 alone and coenzyme Q10 in DMSO were not able to protect cells against oxidative stress.

Prior *in vivo* investigation we checked the stability of loaded polymeric micelles after their incorporation in cream formulation. The stability of HAC18:1 loaded with coenzyme Q10 in o/w cream was checked by a simple extraction test. The cream formulation was diluted with water (1:10 v/v) and shortly centrifuged so that oil cream phase forming the top phase was separated from aqueous phase remaining at the bottom. Being soluble in aqueous solution, intact polymeric micelles (containing coenzyme Q10) are expected to be found in the bottom (aqueous) phase. Conversely, in case of polymeric micelle disaggregation, coenzyme Q10 will leak out from the micelle core and will appear in the oil phase (top phase after extraction). The exact localization of coenzyme Q10 can be easily visualized (Fig. S12) due its characteristic yellowish color. As it can be seen in Fig. S12, the coenzyme Q10 was located in the oil phase in case of control formulations containing either free coenzyme Q10 or a physical mixture of unencapsulated coenzyme Q10 and HAC18:1. The only formulation, containing coenzyme Q10 in water phase was the cream formulation which contained encapsulated coenzyme Q10 in HAC18:1 polymeric micelles. Thus, the loaded micelles remain intact after incorporation in cream formulation. Similar results were obtained after 1, 2, 6 and 12 month after formulation preparation.

Human volunteers applied the cream formulations containing coenzyme Q10, HAC18:1 and HAC18:1 with loaded coenzyme Q10 once per day for one month. After each week of application skin hydration, elasticity, and TEWL were tested. There was no significant difference noticed for elasticity and TEWL. However, a noticeable difference was determined for skin hydration for the formulation containing HAC18:1 with encapsulated coenzyme Q10.

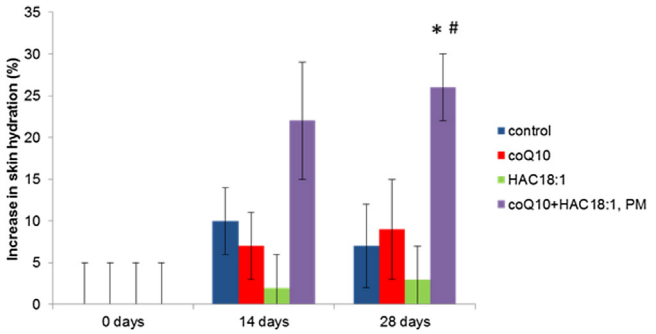

Fig. 7. Increase in skin hydration after application of cream formulation without any additives (control) and added with (i) coenzyme Q10 (coQ10), (ii) HAC18:1 and (iii) coQ10 loaded in HAC18:1 polymeric micelles (coQ10 + HAC18:1, PM). n = 6, * $p < 0.05$ comparing coQ10 and coQ10 loaded in HAC18:1.# $p < 0.05$ comparing HAC18:1 and coQ10 loaded in HAC18:1.

The skin hydration was 2–3 times larger compared to control formulations with none or free coenzyme Q10 or with a formulation containing only HAC18:1 (Fig. 7).

4. Discussion

The fluorescence (Figs. 1 and 3) and confocal images (Figs. Fig. 4 and S8) obtained *in vitro* from excised porcine skin mounted in Franz diffusion cells allowed the following conclusions to be drawn: (a) the skin penetration of loaded hydrophobic compounds in HAC6 and HAC18:1 polymeric micelles is enhanced by hydrophobized HA, (b) modified HA by itself penetrates into deeper skin layers, (c) the penetration route of the associated hydrophobic drug is preferentially transcellular and (d) the hydrophobic drug is released in keratinocytes in epidermis and fibroblasts in dermis.

Topical permeation of most drugs and actives into inner skin layers, in particular dermis, is important to mediate their activity (Scalia, Trotta, Iannuccelli, & Bianchi, 2015). Thus, it is important that HA polymeric micelles are able to enhance delivery of hydrophobic compounds through the *stratum corneum* into deeper skin layers and in this way increase their cutaneous availability. Native low molecular weight HA (5 kDa) has been previously shown to enhance skin penetration of both small and large water soluble molecules (Witting et al., 2015). In this work we have demonstrated, that hydrophobized HA is able to enhance penetration of large hydrophobic molecules (Mw 318 and 863 g/mol), despite the fact that any molecule larger than 500 g/mol is generally considered to be impermeable through the skin (Williams & Barry, 2004). However, the molecular weight of hydrophobic molecule seem to play a role in penetration depth. The HA polymeric micelles enhanced the Nile Red penetration to dermis, but the larger coenzyme Q10 molecules were detected only in the upper epidermis. In addition, acylated HA by itself was found to penetrate the epidermis. Although it seems unlikely due to its large Mw (15,000 g/mol) and high hydrophilicity, this finding is in agreement with previous studies (Brown, Alcorn, & Fraser, 1999; Witting et al., 2015). In case of low molecular weight native HA, the penetration mechanism is still not well understood, and is attributed to the twisted HA conformation containing hydrophobic patches (Brown, Alcorn, & Fraser, 1999) or skin hydration effect connected with keratin conversion from α-helical structure to β-sheet (Witting et al., 2015). In our case, the conversion of the secondary structure of keratin was excluded.

One of the obstacles for HA penetration was expected to be the large hydrodynamic size (diameters from 120 to 230 nm) determined for the loaded vehicles. Drug delivery vehicles with such hydrodynamic size may facilitate skin drug penetration, but at the same time they are not expected to penetrate skin by themselves

unless they are elastic and deformable (Elsayed, Abdallah, Naggar, & Khalafallah, 2007; Gillet, Lecomte, Hubert, Ducat, Evrard, & Piel, 2011). For example, rigid polystyrene nanoparticles with diameters larger than 30 nm were unable to penetrate beyond the *stratum corneum* (Wu, Price, & Guy, 2009).

The overall negative charge of the polymeric micelles arising from dissociated HA carboxyl groups was theoretically expected to lead to charge repulsion between negatively charged *stratum corneum* and cell membranes and favor extracellular pathways, as it was observed in case of negatively charged PAMAM dendrimers (Yang et al., 2012). Charged repulsions, between carboxylate groups and the cell membranes, were believed to force the dendrimers to take extracellular routes, allowing their rapid diffusion (Yang et al., 2012). However, acylated HA forming HA vehicles, as well as the associated hydrophobic compounds, were found to take predominantly the transcellular pathway. Thus, in case of acylated HA, charge repulsion is not the major driving force for the determination of preferential skin permeation route.

The confocal images (Fig. 4) further suggested cotransport of HA vehicle and hydrophobic dye. However, when FRET pair dyes were loaded in HA polymeric micelles and these micelles were incubated with skin in Franz diffusion cells, gradual polymeric micelle disruption starting in the *stratum corneum* and continuing with increasing skin depth was observed (Fig. 5). Therefore, although the fluorescence of NR (non-covalently loaded in polymeric micelles) and Nile Blue (covalently linked via a stable C—N bond to HAC18:1) was detected in the same compartments of both the epidermis and dermis, the FRET data are suggesting micelle disaggregation in upper epidermal layer and separate penetration of the vehicle and the loaded compound. In any case, the HA vehicle significantly enhances penetration of the loaded drug through the *stratum corneum* and at certain point it disaggregates and releases its payload. According to our unpublished data, HAC18:1 is not hydrolyzed under these experimental conditions. Therefore, disaggregation of the micelle due to the enzymatic cleavage of the ester bond between HA and acyl chain can be, in this case, ruled out.

Porcine skin was used for *in vitro* skin penetration studies because it is a good substitute of human skin having similar epidermal thickness, lipid composition, permeability, transepidermal water loss and low frequency impedance (Wu, Price, & Guy, 2009). Unfortunately, sometimes *in vitro* results using animal skin mounted in Franz diffusion are not representative of the actual application *in vivo* (Scalia, Trotta, Iannuccelli, & Bianchi, 2015). For this reason, HA loaded vehicles with coenzyme Q10 were incorporated in cream formulation, and after ensuring about the micelle stability in the cream formulation in time (Fig. S12), the cream was applied once per day for a period of one month by human volunteers. Despite this short application time, a clear benefit of loaded polymeric micelles in skin hydration was observed. Hydrated skin is less prone to wrinkle formation, which is an important aspect of nowadays cosmetic approaches. The skin hydration effect was not observed for the same formulation added either with free coenzyme Q10 or HA vehicle alone, thus supporting the importance of bioavailability improvement of topically applied compounds. Moreover, HA polymeric micelles also improved *in vitro* bioactivity of the loaded drug, particularly antioxidant activity in case of loaded coenzyme Q10 (Fig. S11). This enhancing effect is probably connected with higher retention of coenzyme Q10 in cells when loaded in polymeric micelles (Liu et al., 2011). These observations, together with the conclusions by Sohal et al. (Sohal et al., 2006) that the dietary supplementation of coenzyme Q10 is insufficient to elevate the antioxidative defenses in tissues, suggest that topical delivery with good penetrability may be more efficient in replenishing the bioactivity of coenzyme Q10 in human skin.

5. Conclusion

HA polymeric micelles enhance skin permeation of loaded compounds. Although the mechanism by which these micelles induce such an effect is not known, the observed data suggest micellar disruption in the topmost skin layers, accompanied by drug release and drug and vehicle penetration into deeper epidermal and dermal layers. The predominant penetration pathway, for both, the HA vehicle and the payload, is transcellular. The HAC18:1 polymeric micelles were also found to improve *in vitro* and *in vivo* bioactivity of the payload. These micelles are stable after incorporation in o/w cream formulations, and thus represent great potential for topical delivery systems of apolar cosmetic and pharmaceutical compounds.

Acknowledgments

The authors are thankful to Miroslava Brunclikova from Academy of Science (Institute of Macromolecular Chemistry, Prague) for Golden Gate-ATR analysis.

This work was supported by the Internal Funding Agency of the Tomas Bata University in Zlín under Grant IGA/FT/2016/001.

Appendix A. Supplementary data

Supplementary data associated with this article can be found, in the online version, at http://dx.doi.org/10.1016/j.carbpol.2016.09.013.

References

Bolzinger, M. A., Briancon, S., & Chevalier, Y. (2011). Nanoparticles through the skin: Managing conflicting results of inorganic and organic particles in cosmetics and pharmaceutics. *Wiley Interdisciplinary Reviews: Nanomedicine and Nanobiotechnology*, *3*(5), 463–478.

Brown, M. B., & Jones, S. A. (2005). Hyaluronic acid: A unique topical vehicle for the localized delivery of drugs to the skin. *Journal of the European Academy of Dermatology and Venereology*, *19*(3), 308–318.

Brown, T. J., Alcorn, D., & Fraser, J. R. (1999). Absorption of hyaluronan applied to the surface of intact skin. *Journal of Investigative Dermatology*, *113*(5), 740–746.

Chen, H., Kim, S., He, W., Wang, H., Low, P. S., Park, K., et al. (2008). Fast release of lipophilic agents from circulating PEG-PDLLA micelles revealed by in vivo forster resonance energy transfer imaging. *Langmuir*, *24*(10), 5213–5217.

Cilurzo, F., Vistoli, G., Gennari, C. G., Selmin, F., Gardoni, F., Franze, S., et al. (2014). The role of the conformational profile of polysaccharides on skin penetration: The case of hyaluronan and its sulfates. *Chemistry and Biodiversity*, *11*(4), 551–561.

Contri, R., Fiel, L., Pohlmann, A., Guterres, S., & Beck, R. R. (2011). Transport of substances and nanoparticles across the skin and in vitro models to evaluate skin permeation and/or penetration. In R. Beck, S. Guterres, & A. Pohlmann (Eds.), *Nanocosmetics and nanomedicines* (pp. 3–35). Berlin, Heidelberg: Springer.

Elsayed, M. M., Abdallah, O. Y., Naggar, V. F., & Khalafallah, N. M. (2007). Deformable liposomes and ethosomes as carriers for skin delivery of ketotifen. *Pharmazie*, *62*(2), 133–137.

Gillet, A., Lecomte, F., Hubert, P., Ducat, E., Evrard, B., & Piel, G. (2011). Skin penetration behaviour of liposomes as a function of their composition. *European Journal of Pharmaceutics and Biopharmaceutics*, *79*(1), 43–53.

Huerta-Angeles, G., Bobek, M., Prikopova, E., Smejkalova, D., & Velebny, V. (2014). Novel synthetic method for the preparation of amphiphilic hyaluronan by means of aliphatic aromatic anhydrides. *Carbohydrate Polymers*, *111*, 883–891.

Karande, P., & Mitragotri, S. (2009). Enhancement of transdermal drug delivery via synergistic action of chemicals. *Biochimica Et Biophysica Acta (BBA) – Biomembranes*, *1788*(11), 2362–2373.

Kaushik, D., Costache, A., & Michniak-Kohn, B. (2010). Percutaneous penetration modifiers and formulation effects. *International Journal of Pharmaceutics*, *386*(1–2), 42–51.

Kong, M., Chen, X. G., Kweon, D. K., & Park, H. J. (2011). Investigations on skin permeation of hyaluronic acid based nanoemulsion as transdermal carrier. *Carbohydrate Polymers*, *86*(2), 837–843.

Lapteva, M., Mondon, K., Möller, M., Gurny, R., & Kalia, Y. N. (2014). Polymeric micelle nanocarriers for the cutaneous delivery of tacrolimus: A targeted

approach for the treatment of psoriasis. *Molecular Pharmaceutics*, *11*(9), 2989–3001.
Lauterbach, A., & Müller-Goymann, C. C. (2014). Comparison of rheological properties, follicular penetration, drug release, and permeation behavior of a novel topical drug delivery system and a conventional cream. *European Journal of Pharmaceutics and Biopharmaceutics*, *88*(3), 614–624.
Lee, W.-C., & Tsai, T.-H. (2010). Preparation and characterization of liposomal coenzyme Q10 for in vivo topical application. *International Journal of Pharmaceutics*, *395*(1–2), 78–83.
Liu, J., Pang, Y., Huang, W., Zhu, Z., Zhu, X., Zhou, Y., et al. (2011). Redox-responsive polyphosphate nanosized assemblies: A smart drug delivery platform for cancer therapy. *Biomacromolecules*, *12*(6), 2407–2415.
Manca, M. L., Castangia, I., Zaru, M., Nacher, A., Valenti, D., Fernandez-Busquets, X., et al. (2015). Development of curcumin loaded sodium hyaluronate immobilized vesicles (hyalurosomes) and their potential on skin inflammation and wound restoring. *Biomaterials*, *71*, 100–109.
Papakonstantinou, E., Roth, M., & Karakiulakis, G. (2012). Hyaluronic acid: A key molecule in skin aging. *Dermato-Endocrinology*, *4*(3), 253–258.
Podzimek, S., Hermannova, M., Bilerova, H., Bezakova, Z., & Velebny, V. (2010). Solution properties of hyaluronic acid and comparison of SEC-MALS-VIS data with off-line capillary viscometry. *Journal of Applied Polymer Science*, *116*(5), 3013–3020.
Prow, T. W., Grice, J. E., Lin, L. L., Faye, R., Butler, M., Becker, W., et al. (2011). Nanoparticles and microparticles for skin drug delivery? *Advanced Drug Delivery Reviews*, *63*(6), 470–491.
Scalia, S., Trotta, V., Iannuccelli, V., & Bianchi, A. (2015). Enhancement of in vivo human skin penetration of resveratrol by chitosan-coated lipid microparticles. *Colloids Surface B Biointerfaces*, *135*, 42–49.
Scott, J. E., Cummings, C., Brass, A., & Chen, Y. (1991). Secondary and tertiary structures of hyaluronan in aqueous solution, investigated by rotary shadowing-electron microscopy and computer simulation. Hyaluronan is a very efficient network-forming polymer. *Biochemical Journal*, *274*(Pt 3), 699–705.
Smejkalova, D., Nesporova, K., Hermannova, M., Huerta-Angeles, G., Cozikova, D., Vistejnova, L., et al. (2014). Paclitaxel isomerisation in polymeric micelles based on hydrophobized hyaluronic acid. *International Journal of Pharmaceutics*, *466*(1–2), 147–155.
Sohal, R. S., Kamzalov, S., Sumien, N., Ferguson, M., Rebrin, I., Heinrich, K. R., et al. (2006). Effect of coenzyme Q10 intake on endogenous coenzyme Q content, mitochondrial electron transport chain, antioxidative defenses, and life span of mice. *Free Radical Biology & Medicine*, *40*(3), 480–487.
Williams, A. C., & Barry, B. W. (2004). Penetration enhancers. *Advanced Drug Delivery Reviews*, *56*(5), 603–618.
Witting, M., Boreham, A., Brodwolf, R., Vávrová, K., Alexiev, U., Friess, W., et al. (2015). Interactions of hyaluronic acid with the skin and implications for the dermal delivery of biomacromolecules. *Molecular Pharmaceutics*, *12*(5), 1391–1401.
Wu, X., Price, G. J., & Guy, R. H. (2009). Disposition of nanoparticles and an associated lipophilic permeant following topical application to the skin. *Molecular Pharmaceutics*, *6*(5), 1441–1448.
Yang, Y., Bugno, J., & Hong, S. (2013). Nanoscale polymeric penetration enhancers in topical drug delivery. *Polymer Chemistry*, *4*(9), 2651–2657.
Yang, Y., Sunoqrot, S., Stowell, C., Ji, J., Lee, C. W., Kim, J. W., et al. (2012). Effect of size, surface charge, and hydrophobicity of poly(amidoamine) dendrimers on their skin penetration. *Biomacromolecules*, *13*(7), 2154–2162.